

Article

Enhancing the Photocatalytic Activity of TiO₂ for the Degradation of Congo Red Dye by Adjusting the Ultrasonication Regime Applied in Its Synthesis Procedure

Elvira Turcu ^{1,2}, Cristina Giorgiana Coromelci ^{1,3}, Valeria Harabagiu ² and Maria Ignat ^{1,2,*}¹ Department of Chemistry, “Alexandru Ioan Cuza” University, 11 Carol I Blvd., 700506 Iasi, Romania² “Petru Poni” Institute of Macromolecular Chemistry, 41A Grigore Ghica Voda Alley, 700487 Iasi, Romania³ Department of Exact Sciences and Natural Sciences, Institute of Interdisciplinary Research, “Alexandru Ioan Cuza” University, 11 Carol I Blvd, 700506 Iasi, Romania

* Correspondence: maria.ignat@uaic.ro or ignat.maria@icmpp.ro

Abstract: Recently, the ultrasound-assisted sol-gel synthesis procedure of mesoporous titania (TiO₂) photocatalysts caught the researcher’s attention, due to the physicochemical properties enhancement of the resulting titania nanomaterials. Thus, by varying different synthesis parameters particular characteristics could be obtained. In the present study, the ultrasound pulse on/off ratio has been considered and the effect of the envisaged parameter on the textural, morphological, and optical features of titania nanomaterial has been investigated. Therefore, X-ray Diffraction (XRD), Fourier-Transform Infrared spectroscopy (FTIR), N₂-sorption measurements, SEM imaging, and UV-Vis Diffuse Reflectance spectroscopy (UVDR) have been used. And further, the photocatalytic activity of the prepared TiO₂ materials was evaluated by the features developed about the applied ultrasound pulse on/off ratio as 1/1, 2/1, 3/1, 4/1, 1/3 and 2/2. It was found that the ultrasound pulse on/off ratio considered in the synthesis procedure of titania leads to TiO₂ materials with different textural ($S_{BET} = 98\text{--}156\text{ m}^2/\text{g}$), morphological, and optical ($E_g = 3.1\text{--}3.2\text{ eV}$) characteristics. For this reason, TiO₂ nanomaterials prepared were found to exhibit suitable features for photocatalytic applications. Thus, the TiO₂ 4.1 sample prepared at 4/1 ultrasound pulse on/off ratio revealed the highest photodegradation efficiency of Congo Red dye (98.28%) as the results of photocatalytic tests show. More than that, a possible reaction mechanism of the CR photodegradation process through the contribution of reactive oxygen species ($\cdot\text{HO}$, $\cdot\text{O}_2^-$), holes (h^+), and electrons (e^-) of developed titania photocatalyst was proposed.

Keywords: TiO₂ synthesis; ultrasonication regime; physicochemical properties; photocatalytic performance



Citation: Turcu, E.; Coromelci, C.G.; Harabagiu, V.; Ignat, M. Enhancing the Photocatalytic Activity of TiO₂ for the Degradation of Congo Red Dye by Adjusting the Ultrasonication Regime Applied in Its Synthesis Procedure. *Catalysts* **2023**, *13*, 345. <https://doi.org/10.3390/catal13020345>

Academic Editors: Collin G. Joseph, Gianluca Li Puma and Giovanni Palmisano

Received: 29 December 2022

Revised: 28 January 2023

Accepted: 31 January 2023

Published: 3 February 2023



Copyright: © 2023 by the authors. Licensee MDPI, Basel, Switzerland. This article is an open access article distributed under the terms and conditions of the Creative Commons Attribution (CC BY) license (<https://creativecommons.org/licenses/by/4.0/>).

1. Introduction

One of the most serious issues of environmental pollution is rightly considered to be water pollution. The worldwide development of textile, agricultural, and pharmaceutical industrial activities leads to a huge scale of wastewater [1]. The presence of harmful organic compounds in water resources may be a serious concern for aquatic systems and human health [2,3]. Because the textile, dyeing, cosmetics, plastics, and pharmaceutical industries use more than 100,000 different types of commercial synthetic dyes, and as their annual production exceeds 700,000 tons sustainable solutions to neutralize them from the environment have to be proposed. Since about 15% (100,000 tons) of these dangerous dyes came from textiles industries are reaching into the water due to the inefficient dyeing process [4], their presence in water shows high solubility, toxicity, and stability and as a result, could have a negative effect on ecosystems. Nevertheless, the common techniques such as adsorption, biological degradation, and chemical oxidation didn’t show the expected efficiency in their removal.

In recent years, several techniques are investigated to remove organic contaminants for wastewater remediation among which photocatalysis showed large opportunities due to the low energy consumption, complete decomposition of organic pollutants, and high stability [5–7]. Therefore, many types of photocatalysts have been proposed, investigated, and tested for the removal of such pollutants [8,9]. One of the most interesting photocatalysts that caught researchers' attention is titania (TiO_2), an ideal semiconductor exhibiting special characteristics such as high thermal and chemical stability, being environmentally friendly, and non-toxic [10]. Thereby, titania nanomaterials are used as photocatalysts with excellent wide-bandgap (3.2 eV), and adequate structural, textural, and morphological characteristics exhibiting an oxidizing potential against organic pollutants [10,11]. Such material has been proved to be activated usually by UV-light, but in some cases, the activation could be done by visible light when TiO_2 electronic structure is modified by various dopants that allow shifting the band-gap energy to lower values [12]. Recently, various mesoporous TiO_2 photocatalysts found their applications in catalysis, biological medicine, and green energy [13,14]. Such nanomaterials are obtained through the sol-gel, hydrothermal, solvothermal, and template methods. By varying the synthesis parameters, it may represent an attractive strategy for tailoring the titania nanomaterial features and optimizing them to improve its characteristics. The sol-gel technique is the most frequently used, versatile, and advantageous method, that allows preparing titania material exhibiting different features. Thus, by applying the sol-gel technique and selecting the appropriate conditions, a variety of new mesoporous titania materials with advanced properties could be obtained [13]. Recently, the ultrasound-assisted sol-gel procedure has been reported in the literature elsewhere [11], as an alternative method involving ultrasonic waves to initiate both physical and chemical processes due to cavitation bubble collapse. Thus, when the liquid solution is irradiated by ultrasonic waves, the acoustic cavitation becomes responsible for the anisotropic growth of nanocrystals, for the surface area increase and porosity enhancement [13,15,16].

Since our previous work reports an interesting study regarding the features design of mesoporous titania involving the developed ultrasound-assisted sol-gel method, where the effect of surfactant/titania precursor weight ratio has been considered as a tailoring parameter, the novelty of this study stress on another important parameter to be modified during the synthesis procedure, namely the ultrasonication regime. Thus, in the present study, the effect of the ultrasonication regime on the physicochemical properties of mesoporous titania photocatalysts is reported. Therefore, various on/off acoustic cavitation pulse regimes were considered in the ultrasound-assisted synthesis procedure of titania photocatalyst. The as-synthesized TiO_2 samples were investigated from a structural, textural, morphological, and optical point of view, using various techniques such as X-ray Diffraction (XRD), Fourier-transform infrared spectroscopy (FTIR), N_2 -sorption measurements, SEM imaging, UV-Vis Diffuse Reflectance spectroscopy (UVDR). Withal, the photocatalytic performance of the produced titania materials was evaluated by testing them in a photodegradation reaction of Congo Red (CR) dye, as a model organic pollutant, under UV light irradiation. A possible reaction mechanism was set up by using trapping reagents, such as isopropyl alcohol (IPA), hydroquinone (HQ), ethylenediaminetetraacetic acid (EDTA), and potassium chromate, in the photocatalytic experiments.

2. Results and Discussions

2.1. Characterization of the Synthesized Titania Samples

2.1.1. XRD Measurements

X-ray diffraction patterns of the synthesized titania nanomaterials with ascending "on" cycle and keeping the same, then increasing "off" cycle of ultrasonication regime are represented in Figure 1a and the alternant on/off cycle as shown in Figure 1b. All samples exhibit characteristic peaks corresponding to titanium oxide material, having the maximum intensities at the following diffraction angles: 25.4° , 38° , 48° , 54° , 55.2° , 62.8° , 69.14° , 70.18° , and 75.2° that are associated with (101), (004), (200), (105), (211), (204), (116), (220) and

(215) diffraction planes of main anatase phase [17]. This affirmation is in good agreement with JCPDS 21-1272 characterizing the crystalline anatase tetragonal phase of TiO_2 structure. The observed crystallinity of the prepared oxide structures may be perceived as a great advantage for photocatalytic applications, and not only. At the opposite pole, the literature review shows that the amorphous phase is responsible for the numerous active sites that can act as recombination centers of the photogenerated electron-hole pairs, which imposes serious impediments to the photocatalytic process [18]. On the other hand, as is observed from the recorded diffraction patterns, the ultrasound regime may cause the appearance of a secondary phase, brookite, as an impurity at $2\theta = 31^\circ$ [19,20].

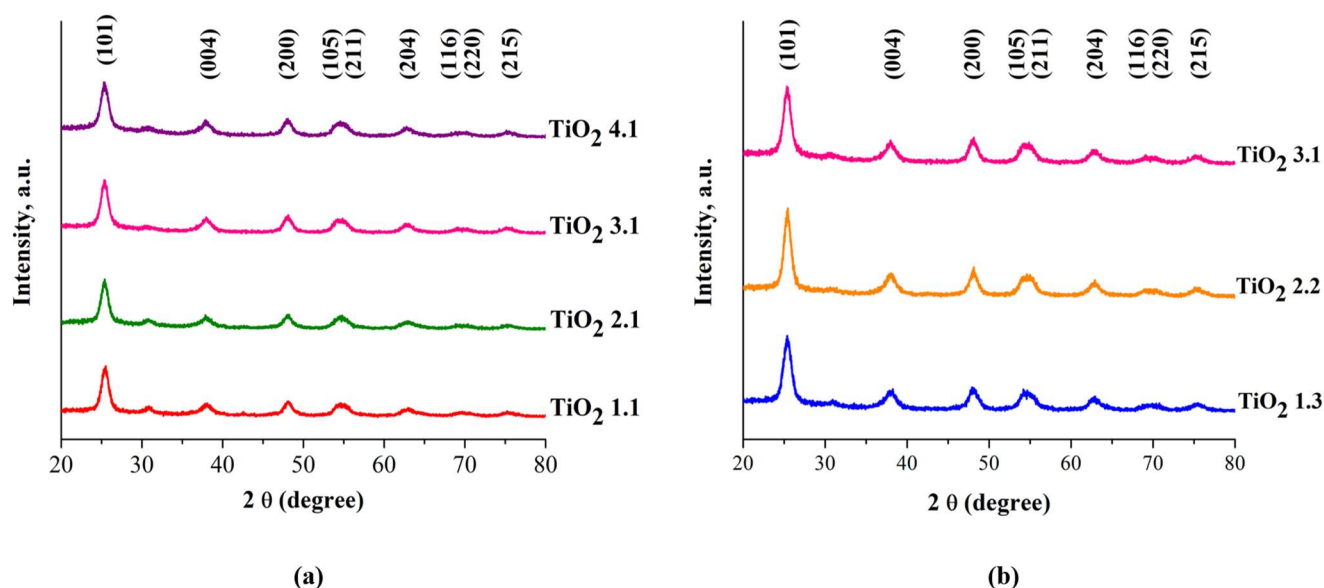


Figure 1. X-ray diffraction patterns for prepared TiO_2 samples by sol-gel techniques applying different ultrasound regimes: (a) by varying on cycle and keeping off cycle constant; (b) by varying both on/off cycles.

The crystallite sizes for the synthesized titania catalysts, according to the Scherrer theory, $D_{Scherrer}$, were found to vary in the range of 7.1–7.9 nm, as revealed in Table 1. These values were compared with commercial P25 titania, whose crystallite size is about four times larger [21]. Considering X-ray data, it is noticeable that the ultrasonication regime applied in the sol-gel synthesis of TiO_2 materials has an improvement effect on the crystallinity. This effect is proved by the Williamson-Hall (W-H) theory allowing to calculate the crystallite sizes, D_{W-H} , which are comparable with $D_{Scherrer}$. Moreover, the W-H plots allowed us to estimate microstrains (ϵ) (Table 1), which values are positive, indicating the synthesized titania samples contain perfect crystals with a slightly expanded lattice. The resulting data reveal that TiO_2 2.2 and TiO_2 3.1 samples exhibit the highest values of $\epsilon = 0.0051$, meaning that the applied ultrasonication regimes are the most suitable on/off cycles for the preparation of TiO_2 nanocrystals.

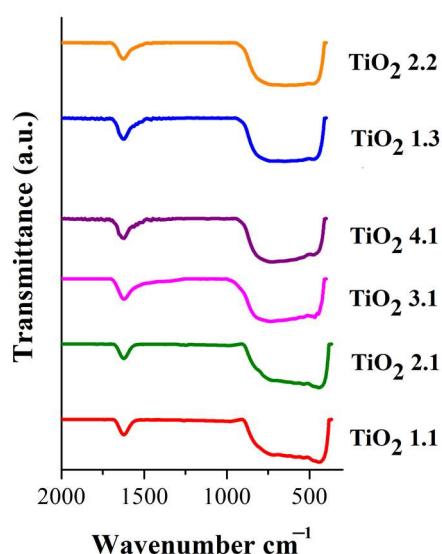
2.1.2. FTIR Investigation of Titania Surface Chemistry

The hydrolysis and condensation reactions during the sol-gel synthesis process led to the formation of TiO_2 nanomaterials as can be seen in Figure 2. Thus, the FTIR spectra for the prepared titania samples after heat treatment at 713.15 K, clearly show two main bands. So then, the band appearing at 1627 cm^{-1} is attributed to the bending vibration of hydroxyl groups (OH) and chemically and physically adsorbed water molecules on the surface due to the strong hydrophilic nature of TiO_2 materials [11,22,23]. The broadest band in the region 895 cm^{-1} – 408 cm^{-1} is assigned to the Ti-O stretching bond characteristic for the TiO_2 anatase phase [11,24].

Table 1. Structural parameters * calculated using XRD data of the prepared titania samples.

Sample ID	2 θ	FWHM	$D_{Scherrer}$ (nm)	D_{W-H} (nm)	$d_{(101)}$ (nm)	a_0 (nm)	ϵ
TiO ₂ 1.1	25.42	1.15	7.8	8.2	0.35	0.40	0.0047
TiO ₂ 2.1	25.37	1.18	7.6	7.0	0.35	0.40	0.0002
TiO ₂ 3.1	25.36	1.23	7.3	8.9	0.35	0.40	0.0051
TiO ₂ 4.1	25.37	1.21	7.4	7.3	0.35	0.40	0.0034
TiO ₂ 1.3	25.38	1.26	7.1	6.7	0.35	0.40	0.0018
TiO ₂ 2.2	25.40	1.13	7.9	9.1	0.35	0.40	0.0051
P25 (commercial) [21]			29.5				

* FWHM—Full Width at Half Maximum for the representative peak of anatase phase (2 θ degree); $D_{Scherrer}$ —crystallite size calculated by using Scherrer formula (nm); D_{W-H} —calculated crystallite size by using Williamson-Hall theory; $d_{(101)}$ —interplanar spacing (nm); a_0 —unit cell parameter (nm); ϵ —lattice strain.

**Figure 2.** Registered Fourier-Transform Infrared (FTIR) spectra for TiO₂ samples synthesized by different ultrasonication regimes.

2.1.3. N₂-Sorption Measurements

As well known, the photocatalytic efficiency of a nanomaterial can be influenced by the textural parameters to the same extent as structural ones [25]. Therefore, the nitrogen adsorption-desorption isotherms were registered to investigate the effect of the ultrasonication regime used in the sol-gel synthesis on the textural features of titania nanomaterials. In this regard, the nitrogen sorption isotherms and the corresponding pore size distributions (inset) for the synthesized samples are represented in Figure 3. According to the IUPAC classification, all adsorption-desorption isotherms are of type IV, characterizing the mesoporous nature of nanomaterials [26]. More than that, the relevant feature of the type IV isotherm is the hysteresis loop, which is correlated with the capillary condensation occurring in mesopores [26–28]. Therefore, the hysteresis loops exhibited by the registered isotherms are of type H2, meaning the pore structure of the synthesized TiO₂ materials is more complex forming a continuous network [26,28]. However, the shape of the hysteresis loop is changing with the ultrasonication regime applied in the synthesis procedure. Thus, the hysteresis loops observed for the TiO₂ 1.3, TiO₂ 2.2, and TiO₂ 3.1 samples are more like an H2(a) type which is due to the very steep desorption branch of isotherm, being associated with the pore blocking (ink-bottle pores) [26], representing the percolation process in a narrow range of pore necks or perhaps to cavitation-induced evaporation [29]. On the other hand, the nitrogen sorption isotherms of TiO₂ 1.1, TiO₂ 2.1, and TiO₂ 4.1 samples are accompanied by an H2(b) hysteresis loop revealing as well the pore blocking with a wider neck size distribution [26,27]. Thus, the BJH PSD plots

for the first series of titania samples (TiO_2 1.3, TiO_2 2.2, and TiO_2 3.1) are narrow compared to PSDs for the second series (TiO_2 1.1, TiO_2 2.1 and TiO_2 4.1) which are wider with the mean pore diameter of larger sizes (Figure 3 (insets)).

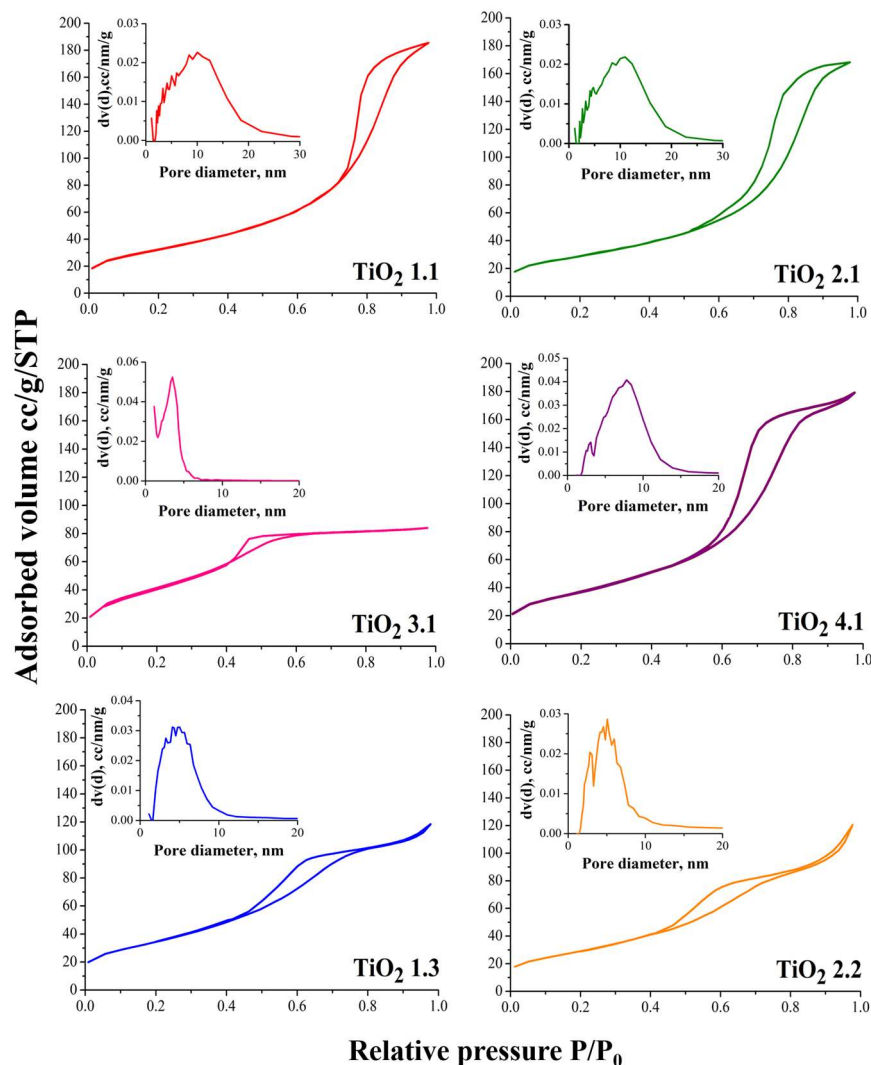


Figure 3. Nitrogen adsorption-desorption isotherms and corresponding BJH pore size distributions (insets) of the synthesized titania materials.

Besides, the nitrogen adsorption isotherms allowed us to calculate the BET-specific surface area (S_{BET}), total pore volume (V_t), and mean pore diameter (d_{pore}) which values are summarized in Table 2. As expected, by applying different ultrasonication regimes during the synthesis of titania, an achievement of distinctive textural features is observed. Thus, Figure 4a reveals that the BET-specific surface area (S_{BET}) of the synthesized catalysts varies as follows: TiO_2 3.1 > TiO_2 4.1 > TiO_2 1.3 > TiO_2 1.1 > TiO_2 2.2 > TiO_2 2.1, being 2–3 times greater than the specific surface area of commercial titania (P25) [21]. Furthermore, it is worth mentioning that by increasing the ultrasonication time (on cycle) and by keeping the lowest break time (off cycle), as in the case of TiO_2 3.1 and TiO_2 4.1 titania samples, it is possible to achieve the highest values for S_{BET} of 156 and 136 m^2/g , respectively, meaning that the used regimes are favorable for high surface area titania. This can be explained by the ultrasonication on/off cycle advantage for the nucleation of the particles in the sol-gel mixture [30]. Moreover, the total pore volume (Figure 4b) and the mean pore diameter (Figure 4c) follow the same trend, TiO_2 3.1 sample exhibiting the lowest values for the two parameters. Therefore, the obtained data indicate that by

increasing the time for “off-cycle” in the ultrasonication regime a decrease in the mean pore diameter of the prepared titania nanomaterials, namely TiO₂ 1.3 and TiO₂ 2.2, could be observed. At the same time, the specific surface area for these two materials seems to be still high, concerning TiO₂ 1.1 and TiO₂ 2.1 samples. Results provide that textural characteristics of mesoporous titania could be controlled by applying different ultrasonication regimes. Compared with literature reports [11,31] the textural features represent an advantage for the photocatalytic process.

Table 2. Textural parameters * resulted from N₂ adsorption-desorption isotherms of synthesized titania samples.

Samples	S _{BET} (m ² /g)	V _{tot} (cm ³ /g)	d _{pore} (nm)
TiO ₂ 1.1	110	0.281	10.02
TiO ₂ 2.1	98	0.259	10.95
TiO ₂ 3.1	156	0.129	3.32
TiO ₂ 4.1	136	0.271	7.95
TiO ₂ 1.3	129	0.174	5.38
TiO ₂ 2.2	109	0.168	6.14
P25 (commercial) [21]	45.7	0.177	7.57

* S_{BET}—specific surface area calculated by using Brunauer–Emmett–Teller theory; V_t—total pore volume estimated from the adsorption branch at a relative pressure of P/P₀ = 0.95; d_{pore}—the mean pore diameter evaluated from BJH-pore size distribution calculated using adsorption branch of isotherm.

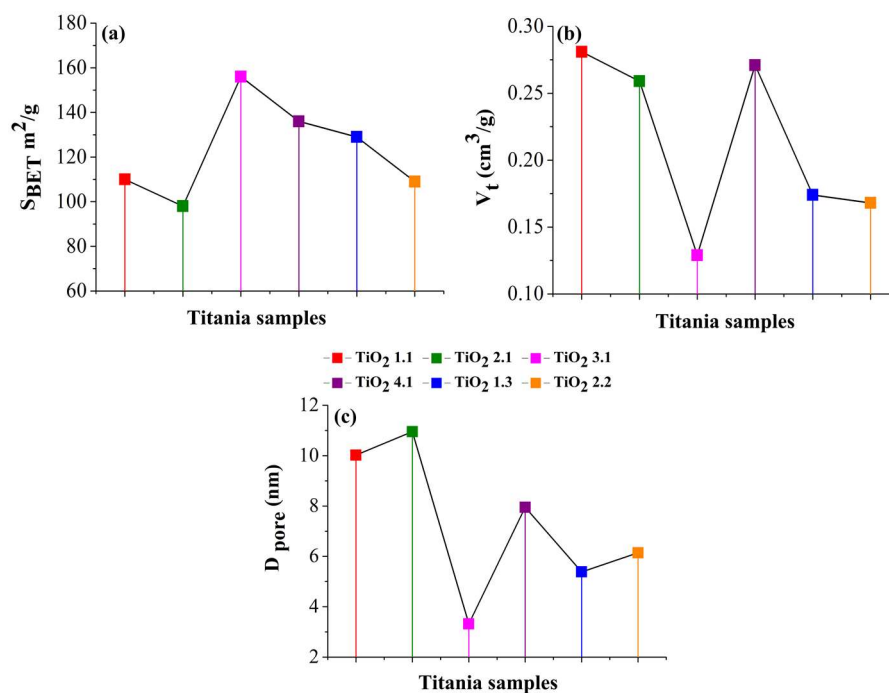


Figure 4. Influence of ultrasonication regime on textural parameters as (a) specific surface area (b) total pore volume and (c) pore size distribution of the prepared titania samples.

2.1.4. Morphology Investigation by SEM

Further, SEM images on the synthesized TiO₂ nanopowders were taken and are shown in Figure 5. A closer look at the registered images reveals an influence of the applied ultrasonication regime on the morphology of newly synthesized titania materials. Thereby, as the “off” cycle of the ultrasonication regime extends, as for TiO₂ 1.3 and TiO₂ 2.2 samples, the TiO₂ particles seem to be more dispersed, revealing a low degree of agglomeration and spherical shapes. On the opposite, when the “on” cycle of the ultrasonication regime is extended, as in the case of TiO₂ 1.1 and TiO₂ 2.1 samples, micrometer-sized structures are observed. While, for TiO₂ 3.1 and TiO₂ 4.1 samples, the morphology of the particles

seems to be more appropriate to TiO₂ 1.3 and TiO₂ 2.2 samples, with an optimum on/off ultrasonication regime of 3/1 for smaller and less agglomerated particles remarking. Thus, to conclude, the ultrasonication process due to the cavitation effect with massive shock waves spread out through a sol, as well as high temperatures, and pressures results in a decrease in theglomeration of TiO₂ nanoparticles [32]. Thereby, according to this finding, the TiO₂ 3.1 and TiO₂ 4.1 samples further could be promising for targeted applications.

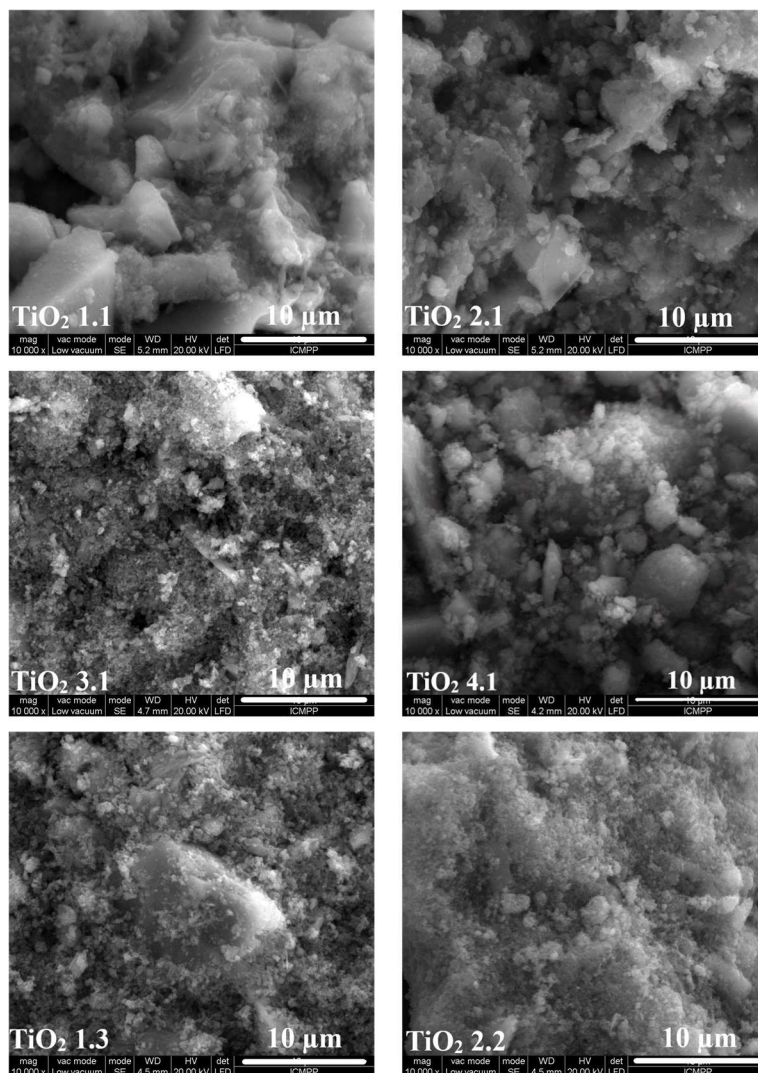


Figure 5. SEM images for the synthesized TiO₂ samples by considering different ultrasonication regimes (magnification 10,000 \times , bar 10 μ m).

2.1.5. Optical Properties Evaluation for the Synthesized Titania Samples

Investigation of optical features of the as-prepared mesoporous titania materials was done by applying the Kubelka-Munk equation to the registered UV-vis DRS spectra. Thus, the drawn Tauc plots [16] in Figure 6 allowed to determine the optical band gap energies (E_g) for each investigated TiO₂ sample. As observed, it was found that the E_g values of the synthesized TiO₂ samples are in the range of 3.1–3.2 eV, characteristic of the anatase phase [11,33,34], being in good agreement with XRD data as well. The found values are lower than that of P25 titania (3.37 eV), as was reported by Wang et al. [21]

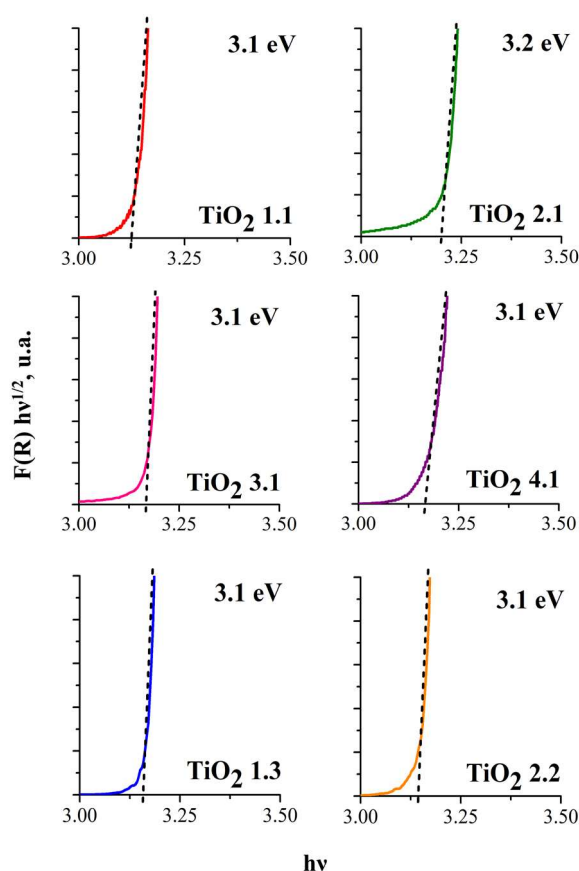


Figure 6. Tauc plots for the synthesized titania materials and their corresponding band gap energies.

2.2. Photocatalytic Degradation of Congo Red Dye

The effect of the ultrasonication regime used in the sol-gel synthesis of titania nano-materials was also investigated from a photocatalytic point of view, of course following highlighted TiO_2 characteristics. For that, the photocatalytic performance of the synthesized titania samples in the CR degradation was evaluated. For clarity, CR photolysis was negligible under the used experimental conditions. Accordingly, the obtained results were plotted and shown in Figure 7a, where the C/C_0 ratio of CR dye vs. time was monitored. As observed, before each photocatalytic test the CR solution was left in contact with the titania samples for 30 min in the dark conditions to achieve the adsorption equilibrium. It was found that an adsorption potential of 40% is proper for the TiO_2 4.1 sample, which is higher than that of the rest of the synthesized samples. According to SEM and BET results, the particles seem to be more dispersed as they exhibit a larger specific surface area, providing more sites for the adsorption process. Further, as observed from Figure 7b, it is notable to mention that the photodegradation efficiency of the TiO_2 4.1 sample in the CR degradation process was (96%) after only 90 min, and reached about 98.28% at a further 30 min. Thereby, the best efficiency for photocatalytic removal of CR dye was found to be given by TiO_2 4.1 which can be explained in terms of favorable textural parameters (specific surface, total pore volume, and pore diameter) that are greater when compared with other as-synthesized TiO_2 samples.

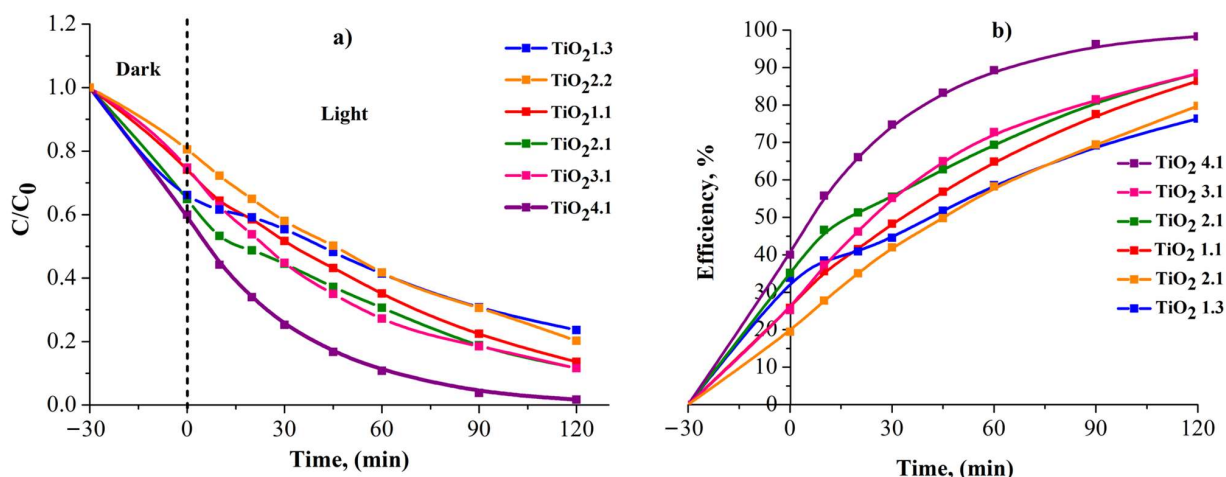


Figure 7. (a) Adsorption in dark conditions and photocatalytic degradation of CR dye under UV-light at equilibrium, (b) removal efficiency of CR dye in the presence of the synthesized titania photocatalysts; note that the initial concentration of CR dye was 50.0 mg/L, and the dosage of TiO₂ catalyst 1 g/L; at a working temperature of $T = 20 \pm 2$ °C.

2.3. Kinetic Study of the Photocatalytic Processes

During the photocatalytic process, the concentration of CR dye was monitored and the results obtained were plotted vs. time and presented in Figure 8. To describe the rate of the decomposition reaction of CR dye over synthesized titania photocatalysts, all experiments were performed under pseudo-first-order (PFO) and pseudo-second-order (PSO) conditions. In this regard, the experimental data characterizing the degradation reaction of CR dye, considering concentration and its variation in time, were fitted first to PFO kinetic model, those that have been expressed as:

$$-\ln \frac{C_t}{C_0} = kt \quad (1)$$

where C_0 is the initial dye concentration at adsorption equilibrium (mg/L), C_t is the concentration of CR dye during UV-light irradiation at time t , k is the pseudo-first-order reaction rate constant (min^{-1}) and t is the irradiation time (min). Considering the corresponding reaction kinetics plots illustrated in Figure 8, the pseudo-first rate constant, k values were estimated from the slope of the fitted lines, and listed in Table 3.

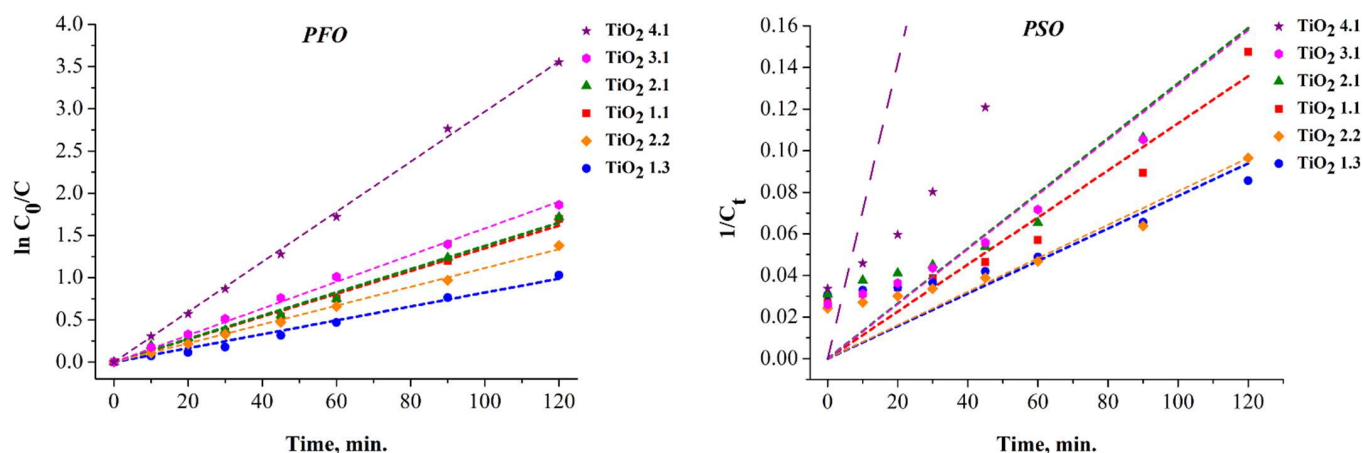


Figure 8. Pseudo-first-order and pseudo-second order photodegradation reaction of CR dye onto titania nanomaterial synthesized under different ultrasonication regimes.

Table 3. The PFO and PSO kinetic rate constants and corresponding regression coefficients resulted in CR dye photodegradation reaction over the synthesized titania samples.

Samples	PFO		PSO		Efficiency (%)
	Rate Constant ($k \times 10^{-2}$, min^{-1})	Regression Coefficient (R^2)	Rate Constant ($k \times 10^{-2}$, min^{-1})	Regression Coefficient (R^2)	
TiO ₂ 1.1	1.4	0.9946	0.08	0.9126	86.42
TiO ₂ 2.1	1.3	0.9922	0.09	0.9125	88.35
TiO ₂ 3.1	1.5	0.9978	0.1	0.9487	88.39
TiO ₂ 4.1	3.0	0.9986	0.67	0.8359	98.28
TiO ₂ 1.3	0.8	0.9925	0.04	0.9606	76.36
TiO ₂ 2.2	1.1	0.9977	0.05	0.9435	79.76

However, the experimental data fit very well with the PFO model, the PSO model was used to make sure there is no doubt over the PFO kinetics reaction. Thus, the calculated regression coefficients (R^2) and rate constants (k) are listed in Table 3, comparatively. As observed, the regression coefficient values (R^2) reveal that the photodegradation kinetics of CR dye is more accurately described by the pseudo-first-order kinetic equation rather than the pseudo-second-order equation. As well, the PFO rate constant appears to be up to 22 times higher than the PSO rate constant, and two times higher than the constant rate of commercial P25 titania (6.02×10^{-3}) [21]. According to findings derived from Figure 7b, the ultrasonication regime appears to influence the photocatalytic performance of the prepared titania material. Therefore, analyzing the evolution of rate constant, for the degradation reaction of CR dye over the synthesized photocatalysts, with the ultrasonication regime applied in the synthesis procedure, the following samples order is created: $k_{\text{TiO}_2 4.1} > k_{\text{TiO}_2 3.1} > k_{\text{TiO}_2 1.1} > k_{\text{TiO}_2 2.1} > k_{\text{TiO}_2 2.2} > k_{\text{TiO}_2 1.3}$. As a result, it has to be noted that the TiO₂ 4.1 titania catalyst exhibit a higher rate constant compared to the rest of the catalytic systems, revealing its photocatalytic performance with a highest CR removal efficiency of 98.28%. Accordingly, considering the obtained results it is important to underline that the ultrasonication regime plays an important role in the physicochemical properties assignment to the mesoporous titania material. An important aspect for photocatalysts application is considered to be its reusability. Thus, the reusability experiments of TiO₂ 4.1 sample for four photocatalytic cycles has been performed, and found that the removal efficiency of CR from the solution decreased to 70%, as could be seen in the Figure S2.

2.4. Trapping Experiments of Active Species in the CR Photodegradation Reaction onto Synthesized Mesoporous Titania Samples

The photodegradation reaction of CR dye was investigated by trapping experiments employing isopropyl alcohol (IPA), hydroquinone (HQ), ethylenediaminetetraacetic acid (EDTA), and potassium chromate (K_2CrO_4) with the role of scavengers for hydroxyl radicals $\cdot\text{HO}$ [35], superoxide $\cdot\text{O}_2^-$ [36], holes h^+ [37] and electrons e^- [38], respectively. The effective contribution of radicals on the degradation of CR dye onto the TiO₂ 4.1 sample can be seen in Figure 9. Thus, one can be concluded that by adding IPA to the photocatalytic system, a significant decrease in the photocatalytic efficiency from 98.28% (no scavenger) to 65.09% (IPA) is observed. This result indicates that $\cdot\text{HO}$ radicals play a major role in the photodegradation process of CR dye onto TiO₂ 4.1 catalyst surface. Further, the presence of HQ and EDTA scavengers led to only a medium decrease in the photocatalytic efficiency from 98.28% (no scavenger) to 69.83% (HQ) and 70.61% (EDTA), respectively. This indicates that the used photocatalytic system contains to the same extent superoxide radicals $\cdot\text{O}_2^-$, and holes h^+ involved in the photodegradation reaction of CR dye. When K_2CrO_4 was introduced in the photocatalytic system as a scavenger, the lowest decrease in the photocatalytic efficiency has been registered, confirming that the electrons e^- play a limited role in CR dye removal by TiO₂ 4.1 catalyst (from 98.28% (no scavenger) to 76.38% (K_2CrO_4)).

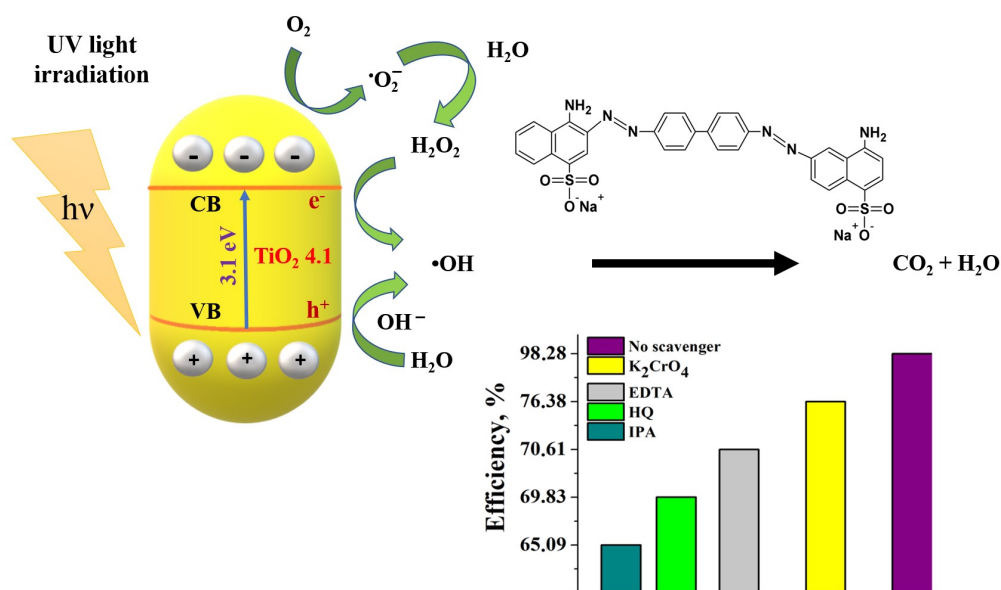


Figure 9. Schematic illustration of CR dye photodegradation mechanism onto TiO₂ 4.1 titania sample and effect of various scavengers on its efficiency.

A schematic mechanism of CR dye photodegradation in an aqueous solution in the presence of TiO₂ 4.1 titania sample is presented as well in Figure 9. Thereby, by absorbing light energy, the electrons from the valence band (VB) are promoted to the conduction band (CB), leaving behind positively charged holes in the VB. With the photogenerated electrons and holes the recombination or the reaction with electron donors or acceptors on the titania photocatalyst surface is possible: formation of hydroxyl radicals $\cdot\text{HO}$ on TiO₂ surface or superoxide anions $\cdot\text{O}_2^-$ in the aqueous environment. These free radicals enable the oxidation process of CR dye onto titania nanoparticles surface [39–41].

3. Materials and Methods

3.1. Materials

Titanium (IV) isopropoxide (TTIP) (C₁₂H₂₈O₄Ti, purity \approx 97%), Pluronic[®] F-127 (PEO₁₀₁-PPO₅₆-PEO₁₀₁) block-copolymer, Congo red dye (C₃₂H₂₂N₆Na₂O₆S₂), and Hydroquinone (C₆H₄(OH)₂) (ReagentPlus \geq 99.5%) were purchased from Sigma-Aldrich Chemie GmbH, Taufkirchen Germany. Isopropyl alcohol (C₃H₈O, \geq 99.7%) and ethylenediaminetetraacetic acid disodium salt (EDTA-Na₂/C₁₀H₁₄N₂Na₂O₈·2H₂O), 99% were obtained from S.C. Chemical Company S.A., Iasi, Romania. All products were analytical grade and used as received.

3.2. Synthesis Procedure of Titania Materials

TiO₂ materials were prepared by the ultrasound-assisted sol-gel method using TTIP as titania precursor and the non-ionic surfactant Pluronic[®] F127, according to reference [42]. In a typical synthesis procedure, the non-ionic surfactant F127 (10 g) was dissolved in a 100 mL water-isopropyl alcohol (1:1) mixture, aided by magnetic stirring. When a clear solution was obtained, titanium tetra-isopropoxide (TTIP) (18 mL) was added dropwise to the surfactant solution in the first 10 min as the ultrasonication process started. The time considered for ultrasonication was 60 min. To evaluate the effect of ultrasound pulse on titania characteristics, various ultrasound pulse on/off ratios were considered, as is revealed in Table 4. The ultrasonication process was achieved using a VibraCell type sonotrode of 750 W power, VCX 750 model (Sonics, Newtown, CT 06470), working at 25% of amplitude. Thereby, the hydrolysis reaction of titanium isopropoxide and the condensation of the resulting titanium hydroxide around surfactant micelles are promoted by ultrasounds. Further, the recovered white precipitates by centrifugation (4000 rpm,

10 min) were washed several times with distilled water, dried at room temperature, and calcined at 713.15 K to burn out the surfactant molecules.

Table 4. Ultrasound pulse on/off ratios varied in the synthesis procedure of TiO₂ materials.

No.	Sample Label	Ultrasounds Pulse ¹	
		On	Off
1	TiO ₂ 1.1	1	1
2	TiO ₂ 2.1	2	1
3	TiO ₂ 3.1	3	1
4	TiO ₂ 4.1	4	1
5	TiO ₂ 1.3	1	3
6	TiO ₂ 2.2	2	2

¹ Ultrasounds pulse on/off unit—seconds.

3.3. Characterization Methods

The effect of ultrasonication pulse on/off ratio on the physicochemical characteristics of the resulted titania samples was investigated in terms of X-ray diffraction (XRD) (Bruker AXS, Karlsruhe, Germany), Fourier Transform Infrared (FTIR) spectroscopy (Bruker Optics, Leipzig, Germany), nitrogen-sorption measurements, Scanning Electron Microscopy (SEM), and UV-diffuse reflectance (UVDR) spectroscopy (Shimadzu, Selm, Germany).

The structural characteristics of the synthesized samples were investigated on a Bruker-AXS: D8 ADVANCE Diffractometer (Bruker AXS, Karlsruhe, Germany) using copper radiation ($\lambda(\text{Cu } K_{\alpha}) = 1.5406 \text{ \AA}$). X-ray diffraction patterns were registered on the synthesized TiO₂ powders in the range of $2\theta = 20 - 80^{\circ}$, using a scanning step of $0.02^{\circ}/s$. The crystallite sizes were calculated using the Scherrer equation [43]:

$$D_{\text{Scherrer}} = \frac{0.94\lambda}{\beta \times \cos \theta_{hkl}} \quad (2)$$

where θ is the diffraction angle, λ —X-ray wavelength, β —full width at half maximum (FWHM) of the considered diffraction peak, and h, k, l are the Miller indices.

The lattice parameter (a_0) was determined by applying the relation:

$$a_0 = 2d/\sqrt{3}, \quad (3)$$

d_{hkl} is the interplanar distance and was calculated using the Bragg equation:

$$d_{hkl} = \frac{\lambda}{2 \sin \theta'} \quad (4)$$

Also, the crystallite sizes of synthesized samples were investigated for comparison with the Williamson-Hall method. Further $\beta \cos \theta$ was plotted vs. $4 \sin \theta$ and from the slope of the fitted line was calculated the strains of each sample were [5,8].

The surface chemistry of analyzed materials was investigated with FTIR spectroscopy. The FTIR spectra were obtained on a Bruker Vertex 70v FTIR spectrometer (Bruker Optics, Leipzig, Germany) at room temperature with a resolution of 2 cm^{-1} in the range of $4000-400 \text{ cm}^{-1}$. All TiO₂ samples have been analyzed by KBr method.

The textural parameters of obtained products were investigated by N₂ sorption on a NOVA 2200e instrument (Quantachrome Corporation, Odelzhausen, Germany). This automated system is using the nitrogen adsorbate at -196°C . First, all synthesized samples were subjected to outgas for 2 h under a high vacuum at room temperature. The specific surface area and the pore size distribution were investigated using the Brunauer-Emmett-Teller (BET) theory, respectively Barrett-Joyner-Halenda (BJH) method. From nitrogen adsorption-desorption isotherms was estimated the total pore volume at relative pressure $\frac{P}{P_0} = 0.95$.

The Scanning Electron Microscope type ESEM Quanta 200 (Fei Company, Hillsboro, Oregon, USA) was used for the morphological investigation of the prepared samples.

For investigation of the light absorption properties of titania nanoparticles, diffuse reflectance spectra were performed using a Shimadzu UV-2401 spectrophotometer (Selm, Germany) equipped with an integrating sphere. A sample of MgO was used as a reference. The Kubelka-Munk function ($F(R) = \frac{(1-R)^2}{2R} = \frac{k}{s} = \frac{A \cdot c}{s}$, where R —reflectance, k —absorption coefficient, s —scattering coefficient, c —concentration of absorbing species, A —absorbance and the Tauc plots obtained from diffuse reflectance spectra bring information about band gap energy. The indirect band gap energy values were achieved by extrapolating the linear part of the graphics to the axis of the abscissa.

3.4. Assessing the Photocatalytic Performance

Photocatalytic experiments have been carried out using the Congo Red (CR) dye solution, at a working pH of 5.5. All experiments were accomplished using the irradiation of a UV lamp (Herolab UV Hand Lamp, Herolab GmbH Laborgeräte, Wiesloch, Germany, 15 W) working at two selectable wavelengths ($\lambda_{max} = 365$ nm and 254 nm) which was placed inside a dark environment. The lamp was placed at 15 cm height above sample solutions, where the power density was measured using an HD2102.2 type photoradiometer (Delta Ohm, Caselle di Selvazzano (PD), Italy) equipped with the SICRAM automatic detection module. Thus, the measured power densities for each wavelength are 0.153 mW/cm² and 0.312 mW/cm², for 254 nm and 365 nm, respectively. The photocatalytic tests were carried out by dispersing 0.05 g of each prepared TiO₂ powdered photocatalyst in 50 mL portions of dye solution containing 50 mg L⁻¹ of CR. First, the resulting mixtures were magnetically stirred in dark conditions for 30 min to achieve the adsorption/desorption equilibrium between CR dye molecules and the photocatalyst's surface. Thereafter, the UV lamp was turned on subjecting the suspension to light irradiation, for different time intervals in the same magnetic stirring conditions. At fixed time intervals (0, 5, 10, 15, 20, 30, 45, 60, 90, and 120 min), aliquots (4 mL) of the suspension were collected and filtered through syringe filters (0.45 μ , PTFE Isolab, Wertheim, Germany) and the absorbance of the filtered CR dye solution was registered immediately, by using a Shimadzu UV-Vis 2450 spectrophotometer. The photocatalytic efficiency (E , %) was calculated using Equation (5):

$$E, \% = \frac{(C_0 - C)}{C_0} * 100 \quad (5)$$

The TiO₂ surface characteristics in UV photodegradation of CR dye were investigated through the active species. The effect and contributions of \cdot HO and \cdot O₂⁻ radicals, holes (h^+), and electrons (e^-) in the titania-mediated photocatalytic process were investigated by considering the presence of various trapping reagents in investigated photocatalytic systems, such as isopropyl alcohol (10 mM), hydroquinone (0.25 mM), ethylenediaminetetraacetic acid (EDTA, 0.5 M) and potassium chromate (K₂CrO₄, 0.025 mM) in 50 mg L⁻¹ CR solution containing 0.05 g of titania photocatalyst.

4. Conclusions

In the present study, mesoporous TiO₂ materials were synthesized by an ultrasound-assisted sol-gel method considering different ultrasonication regimes. The as-prepared titania nanomaterials were investigated by XRD measurements, revealing anatase as the main phase. By increasing the "on" cycle of the applied ultrasonication regime the crystallite size decrease was observed (from 7.8 to 7.4 nm). In connection with this, the characteristic band gap energy values (of 3.1–3.2 eV) for the anatase phase, derived from UV-DR diffuse reflectance spectra, have been proved. Moreover, FTIR measurements showed the main broadest band (895 cm⁻¹–408 cm⁻¹) characteristic for Ti-O stretching of TiO₂ anatase phase. Even more, the time increasing at the "on" cycle, higher specific surface areas of TiO₂ photocatalyst could be achieved (156 and 136 m²/g for TiO₂ 3.1 and TiO₂ 4.1 samples, respectively). Between these two, although TiO₂ 3.1 sample exhibited the highest surface

area, TiO₂ 4.1 sample showed the highest pore volume, which enable it to host more species. Thus, it was proved that the prepared titania sample by applying a 4on/1off ultrasonication regime (TiO₂ 4.1) exhibits the optimized physicochemical properties that recommend it for further photocatalytic applications. This sample exhibits ink-bottle pores where the neck widths are much larger than the neck of other here-synthesized samples. Further, the synthesized samples have been tested in a photodegradation reaction of CR dye under UV irradiation. And as expected, TiO₂ 4.1 synthesized titania sample proved to be the most performant photocatalyst, revealing the maximum efficiency removal of 98.28%. Moreover, it was concluded that the best ultrasonication regime (4on/1off) used in the synthesis procedure of titania nanomaterial, led to the highest PFO rate constant in the degradation process of CR dye ($k = 3.0 \times 10^{-2}$, min⁻¹). Besides, a schematic diagram of the possible photocatalytic mechanism of CR dye onto TiO₂ 4.1 catalyst was designed, as the result of various scavengers involved. Thus, the IPA scavenger led to a significant decrease in the removal efficiency of CR dye (from 98.28% (no scavenger) to 65.09% (IPA)), concluding that ·HO radicals are the main responsible produced reactive oxygen species for the photodegradation process. Likewise, the investigations regarding the reusability of TiO₂ 4.1 sample revealed that the high efficiency is still maintained (92–70%) after four consecutive cycles of photocatalytic degradation of CR dye.

Supplementary Materials: The following supporting information can be downloaded at: <https://www.mdpi.com/article/10.3390/catal13020345/s1>, Figure S1: UVDR spectra for the synthesized titania samples, considering various ultrasonication regimes; Figure S2: The reusability of TiO₂ 4.1 sample for four cycles of application for CR photodegradation; Figure S3: FTIR spectra of TiO₂ 4.1 sample before and after photodegradation test of CR dye.

Author Contributions: Conceptualization, M.I. and E.T.; methodology, M.I.; software, E.T.; validation, M.I. and V.H.; formal analysis, E.T. and C.G.C.; investigation, E.T. and C.G.C.; resources, M.I.; data curation, M.I.; writing—original draft preparation, E.T.; writing—review and editing, C.G.C.; visualization, V.H.; supervision, M.I.; project administration, M.I.; funding acquisition, M.I. All authors have read and agreed to the published version of the manuscript.

Funding: This research was funded by a grant from the Ministry of Research and Innovation, CNCS-UEFISCDI, project number PN-III-P1-1.1-TE-2016-0805, within PNCDI III.

Data Availability Statement: Not applicable.

Acknowledgments: Florica Doroftei is acknowledged for helping with SEM image acquisition.

Conflicts of Interest: The authors declare no conflict of interest. The funders had no role in the design of the study; in the collection, analyses, or interpretation of data; in the writing of the manuscript; or in the decision to publish the results.

References

1. Murgolo, S.; Ceglie, C.D.; Iaconi, C.D.; Mascolo, G. Novel TiO₂-based catalysts employed in photocatalysis and photoelectrocatalysis for effective degradation of pharmaceuticals (PhACs) in water: A short review. *Curr. Opin. Green Sustain. Chem.* **2021**, *30*, 100473. [[CrossRef](#)]
2. Samoila, P.; Cojocaru, C.; Mahu, E.; Ignat, M.; Harabagiu, V. Boosting catalytic wet-peroxide-oxidation performances of cobalt ferrite by doping with lanthanides for organic pollutants degradation. *J. Environ. Chem. Eng.* **2021**, *9*, 104961. [[CrossRef](#)]
3. Chen, D.; Cheng, Y.; Zhou, N.; Chen, P.; Wang, Y.; Li, K.; Huo, S.; Cheng, P.; Peng, P.; Zhang, R.; et al. Photocatalytic degradation of organic pollutants using TiO₂-based photocatalysts: A review. *J. Clean. Prod.* **2020**, *268*, 121725. [[CrossRef](#)]
4. Nur, A.S.M.; Sultana, M.; Mondal, A.; Islam, S.; Nur Robel, F.; Islam, A.; Sumi, M. A review on the development of elemental and codoped TiO₂ photocatalysts for enhanced dye degradation under UV-vis irradiation. *J. Water Process Eng.* **2022**, *47*, 102728. [[CrossRef](#)]
5. Wang, Q.; Zhao, Y.; Zhang, Z.; Liao, S.; Deng, Y.; Wang, X.; Ye, Q.; Wang, K. Hydrothermal preparation of Sn₃O₄/TiO₂ nanotube arrays as effective photocatalysts for boosting photocatalytic dye degradation and hydrogen production. *Ceram. Int.* **2023**, *49*, 5977–5985. [[CrossRef](#)]
6. Liu, C.; Mao, S.; Shi, M.; Wang, F.; Xia, M.; Chen, Q.; Ju, X. Peroxymonosulfate activation through 2D/2D Z-scheme CoAl-LDH/BiOBr photocatalyst under visible light for ciprofloxacin degradation. *J. Hazard. Mater.* **2021**, *420*, 126613. [[CrossRef](#)] [[PubMed](#)]

7. Liu, C.; Mao, S.; Shi, M.; Hong, X.; Wang, D.; Wang, F.; Xia, M.; Chen, Q. Enhanced photocatalytic degradation performance of BiVO₄/BiOBr through combining Fermi level alteration and oxygen defect engineering. *Chem. Eng. J.* **2022**, *449*, 137757. [[CrossRef](#)]
8. Ali, S.; Nasir, J.A.; Dara, R.N.; Rehman, Z. Modification strategies of metal oxide photocatalysts for clean energy and environmental applications: A review. *Inorg. Chem. Commun.* **2022**, *145*, 110011. [[CrossRef](#)]
9. Madima, N.; Kefeni, K.K.; Mishra, S.B.; Mishra, A.K.; Kuvarega, T.A. Fabrication of magnetic recoverable Fe₃O₄/TiO₂ heterostructure for photocatalytic degradation of rhodamine B dye. *Inorg. Chem. Commun.* **2022**, *145*, 109966. [[CrossRef](#)]
10. Roy, J. The synthesis and applications of TiO₂ nanoparticles derived from phytochemical sources. *J. Ind. Eng. Chem.* **2022**, *106*, 1–19. [[CrossRef](#)]
11. Mahu, E.; Coromelci, C.G.; Lutic, D.; Asaftei, I.V.; Sacaescu, L.; Harabagiu, V.; Ignat, M. Tailoring mesoporous titania features by ultrasound-assisted sol-gel technique: Effect of surfactant / titania precursor weight ratio. *Nanomaterials* **2021**, *11*, 1263. [[CrossRef](#)] [[PubMed](#)]
12. Etacheri, V.; Di Valentin, C.; Schneider, J.; Bahnemann, D.; Pillai, S.C. Visible-light activation of TiO₂ photocatalysts: Advances in theory and experiments. *J. Photochem. Photobiol C Photochem. Rev.* **2015**, *25*, 1–29. [[CrossRef](#)]
13. Niu, B.; Wang, X.; Wu, K.; He, X.; Zhang, R. Mesoporous Titanium Dioxide: Synthesis and Applications in Photocatalysis. *Materials* **2018**, *11*, 1910. [[CrossRef](#)] [[PubMed](#)]
14. Kazachenko, A.S.; Vasilieva, N.Y.; Fetisova, O.Y.; Sychev, V.V.; Elsuf'ev, E.V.; Malyar, Y.N.; Issaoui, N.; Miroshnikova, A.V.; Borovkova, V.S.; Kazachenko, A.S.; et al. New reactions of betulin with sulfamic acid and ammonium sulfamate in the presence of solid catalysts. *Biomass Convers. Biorefinery* **2022**, 1–12. [[CrossRef](#)]
15. Giannakoudakis, D.A.; Lomot, D.; Colmenares, J.C. When sonochemistry meets heterogeneous photocatalysis: Designing a sonophotoreactor towards sustainable selective oxidation. *Green Chem.* **2020**, *22*, 4896–4905. [[CrossRef](#)]
16. Coromelci-Pastravanu, C.; Ignat, M.; Popovici, E.; Harabagiu, V. TiO₂ -coated mesoporous carbon: Conventional vs. microwave-annealing process. *J. Hazard. Mater.* **2014**, *278*, 382–390. [[CrossRef](#)]
17. Zhao, H.; Cui, S.; Li, G.; Li, N.; Li, X. 1T- and 2H-mixed phase MoS₂ nanosheets coated on hollow mesoporous TiO₂ nanospheres with enhanced photocatalytic activity. *J. Colloid Interface Sci.* **2020**, *567*, 10–17. [[CrossRef](#)]
18. Lincho, J.; Gomes, J.; Kobylanski, M.; Bajorowicz, B.; Zaleska-Medynska, A.; Martins, R.C. TiO₂ nanotube catalysts for parabens mixture degradation by photocatalysis and ozone-based technologies. *Process Saf. Environ. Prot.* **2021**, *152*, 601–613. [[CrossRef](#)]
19. Guo, Q.; Wu, J.; Yang, Y.; Liu, X.; Sun, W.; Wei, Y.; Lan, Z.; Lin, J.; Huang, M.; Chen, H.; et al. Low-temperature processed rare-earth doped brookite TiO₂ scaffold for UV stable, hysteresis-free and high-performance perovskite solar cells. *Nano Energy* **2020**, *77*, 105183. [[CrossRef](#)]
20. Rosado, G.; Valenzuela-Muñiz, A.M.; Miki-Yoshida, M.; Ysmael Verde, G. Facile method to obtain anatase and anatase-brookite nanoparticles (TiO₂) with MWCNT towards reducing the bandgap. *Diam. Relat. Mater.* **2020**, *109*, 108015. [[CrossRef](#)]
21. Wang, G.; Xu, L.; Zhang, J.; Yin, T.; Han, D. Enhanced Photocatalytic Activity of TiO₂ Powders (P25) via Calcination Treatment. *Int. J. Photoenergy* **2012**, *2012*, 265760. [[CrossRef](#)]
22. León, A.; Reuquen, P.; Garín, C.; Segura, R.; Vargas, P.; Zapata, P.; Orihuela, P.A. FTIR and Raman Characterization of TiO₂ Nanoparticles Coated with Polyethylene Glycol as Carrier for 2-Methoxyestradiol. *Appl. Sci.* **2017**, *7*, 49. [[CrossRef](#)]
23. Praveen, P.; Viruthagiri, G.; Mugundan, S.; Shanmugam, N. Structural, optical and morphological analyses of pristine titanium di-oxide nanoparticles-synthesized via sol-gel route. *Spectrochim. Acta Part A Mol. Biomol. Spectrosc.* **2014**, *117*, 622–629. [[CrossRef](#)] [[PubMed](#)]
24. Dodoo-Arhin, D.; Buabeng, F.P.; Mwabora, J.M.; Amaniampong, P.N.; Agbe, H.; Nyankson, E.; Obada, D.O.; Asiedu, N.Y. The effect of titanium dioxide synthesis technique and its photocatalytic degradation of organic dye pollutants. *Heliyon* **2018**, *4*, e00681. [[CrossRef](#)] [[PubMed](#)]
25. Gharagozlou, M.; Naghibi, S. Preparation of vitamin B12–TiO₂ nanohybrid studied by TEM, FTIR and optical analysis techniques. *Mater. Sci. Semicond. Process.* **2015**, *35*, 166–173. [[CrossRef](#)]
26. Thommes, M.; Kaneko, K.; Neimark, A.V.; Olivier, J.P.; Rodriguez-Reinoso, F.; Rouquerol, J.; Sing, K.S.W. Physisorption of gases, with special reference to the evaluation of surface area and pore size distribution (IUPAC Technical Report). *Pure Appl. Chem.* **2015**, *87*, 1051–1069. [[CrossRef](#)]
27. Kruk, M.; Jaroniec, M. Gas Adsorption Characterization of Ordered Organic-Inorganic Nanocomposite Materials. *Chem. Mater.* **2001**, *13*, 3169–3183. [[CrossRef](#)]
28. Sing, K.S.W. Reporting Physisorption Data For Gas/Solid Systems with Special Reference to the Determination of Surface Area and Porosity. *Pure Appl. Chem.* **1985**, *57*, 603–619. [[CrossRef](#)]
29. Ravikovitch, P.I.; Neimark, A.V. Experimental Confirmation of Different Mechanisms of Evaporation from Ink-Bottle Type Pores: Equilibrium, Pore Blocking, and Cavitation. *Langmuir* **2002**, *18*, 9830–9837. [[CrossRef](#)]
30. Mahmoud, H.R.; El-molla, S.A.; Naghmash, M.A. Novel mesoporous MnO₂/SnO₂ nanomaterials synthesized by ultrasonic-assisted co-precipitation method and their application in the catalytic decomposition of hydrogen peroxide. *Ultrasonics* **2019**, *95*, 95–103. [[CrossRef](#)]
31. Neppolian, B.; Wang, Q.; Jung, H.; Choi, H. Ultrasonic-assisted sol-gel method of preparation of TiO₂ nano-particles: Characterization, properties and 4-chlorophenol removal application. *Ultrason. Sonochemistry* **2008**, *15*, 649–658. [[CrossRef](#)]

32. Ibrahim, S.M.; Halim, S.A. Novel SnZr oxides nanomaterials synthesized by ultrasonic-assisted co-precipitation method: Application in biodiesel production and DFT study. *J. Mol. Liq.* **2021**, *339*, 116652. [[CrossRef](#)]
33. Ignat, M.; Rotaru, R.; Samoila, P.; Sacarescu, L.; Timpu, D.; Harabagiu, V. Relationship between the component synthesis order of zinc ferrite e titania nanocomposites and their performances as visible light-driven photocatalysts for relevant organic pollutant degradation. *Comptes Rendus Chim.* **2018**, *21*, 263–269. [[CrossRef](#)]
34. Reyes-Coronado, D.; Rodriguez-Gattorno, G.; Espinosa-Pesqueira, M.E.; Cab, C.; de Coss, R.; OSkam, G. Phase-pure TiO₂ nanoparticles: Anatase, brookite and rutile. *Nanotechnology* **2008**, *145605*, 10.
35. Coromelci, C.; Neamtu, M.; Ignat, M.; Samoila, P.; Zaltariov, M.F.; Palamaru, M. Ultrasound assisted synthesis of heterostructured TiO₂/ZnFe₂O₄ and TiO₂/ZnFe_{1.98}La_{0.02}O₄ systems as tunable photocatalysts for efficient organic pollutants removal. *Ceram. Int.* **2022**, *48*, 4829–4840. [[CrossRef](#)]
36. Wu, S.; Hu, H.; Lin, Y.; Zhang, J.; Hu, Y.H. Visible light photocatalytic degradation of tetracycline over TiO₂. *Chem. Eng. J.* **2020**, *382*, 122842. [[CrossRef](#)]
37. Mancuso, A.; Sacco, O.; Vaiano, V.; Sannino, D.; Pragliola, S.; Venditto, V.; Morante, N. Visible light active Fe-Pr co-doped TiO₂ for water pollutants degradation. *Catal. Today* **2021**, *380*, 93–104. [[CrossRef](#)]
38. Perciani de Moraes, N.; Azzoni Torezin, F.; Dantas Viégas Jucá, G.; Giancoli Martins de Sousa, J.; Bertholo Valim, R.; da Silva Rocha, R.; Landers, R.; Caetano Pinto da Silva, M.L.; Alvares Rodrigues, L. TiO₂/Nb₂O₅/carbon xerogel ternary photocatalyst for efficient degradation of 4-chlorophenol under solar light irradiation. *Ceram. Int.* **2020**, *46*, 14505–14515. [[CrossRef](#)]
39. Alshehri, A.; Malik, A.; Maqsood Khan, Z.; Al-Thabaitia, S.A.; Hassan, N. Biofabrication of Fe nanoparticles in aqueous extract of *Hibiscus sabdariffa* with enhanced photocatalytic activities. *RSC Adv.* **2017**, *7*, 25149–25159. [[CrossRef](#)]
40. Chankhanittha, T.; Watcharakitti, J.; Nanan, S. PVP-assisted synthesis of rod-like ZnO photocatalyst for photodegradation of reactive red (RR141) and Congo red (CR) azo dyes. *J. Mater. Sci. Mater. Electron.* **2019**, *30*, 17804–17819. [[CrossRef](#)]
41. Bai, B.; Qiu, L.; Mei, D.; Jin, Z.; Song, L.; Du, P. Firmly-supported porous fabric fiber photocatalysts: TiO₂/porous carbon fiber cloth composites and their photocatalytic activity. *Mater. Res. Bull.* **2022**, *148*, 11672. [[CrossRef](#)]
42. Mahu, E.; Ignat, M.; Cojocar, C.; Samoila, P.; Coromelci, C.; Asaftei, I.; Harabagiu, V. Development of Porous Titania Structure with Improved Photocatalytic Activity: Response Surface Modeling and Multi-Objective Optimization. *Nanomaterials* **2020**, *10*, 998. [[CrossRef](#)] [[PubMed](#)]
43. Cullity, B.D. *Elements of X-Ray Diffraction*, 2nd ed.; Addison Wesley Publishing Company, Inc.: Reading, MA, USA, 1978.

Disclaimer/Publisher’s Note: The statements, opinions and data contained in all publications are solely those of the individual author(s) and contributor(s) and not of MDPI and/or the editor(s). MDPI and/or the editor(s) disclaim responsibility for any injury to people or property resulting from any ideas, methods, instructions or products referred to in the content.